arXiv:astro-ph/0107520v1 27 Jul 2001

High-Resolution X-ray and Radio Observations of SGR 1900+14 in the Immediate Aftermath of a Giant Flare

D. W. Fox, D. L. Kaplan, S. R. Kulkarni

Department of Astronomy, 105-24 California Institute of Technology, Pasadena, California 91125, USA

derekfox@astro.caltech.edu, dlk@astro.caltech.edu, srk@astro.caltech.edu

and

D. A. Frail

National Radio Astronomy Observatory, Socorro, NM 87801, USA

dfrail@nrao.edu

ABSTRACT

We present the results of *Chandra*, *RXTE*, and VLA observations of SGR 1900+14 in the immediate aftermath of its 2001 April 18 giant flare event. In the X-ray band we find the source in a pulsating and bursting state, with time-averaged 2–10 keV flux initially elevated by 20% above the source's previous quiescent periods. In the radio we establish upper limits on the strength of any persistent post-flare emission of 0.7 and 0.1 mJy at 1.4 GHz and 8.0 GHz, respectively. The position of the X-ray source is consistent, to approximately 1 arcsec precision, with the August 1998 VLA determination, and the one-dimensional X-ray profile is consistent with that of a point source. The X-ray spectrum is best-fit by a two component power-law plus blackbody model, with fitted blackbody temperature $kT_{\rm BB} \approx 0.5$ keV and radius $R_{\rm BB} \approx 1.5$ km for an assumed distance of 5 kpc. The spectral parameters of this thermal component are consistent with those reported for the source in quiescence, and the variations in the source flux we observe may be explained as variations in the power-law component alone, providing support for magnetar models of SGR 1900+14.

1. Introduction

The Soft Gamma-Ray Repeaters (SGRs; see Hurley 2000 for a recent observational review) are a unique class of Galactic neutron stars that exhibit bright flaring activity in the

hard X-ray and soft gamma-ray bands. Perhaps their most unusual and distinctive feature is their hyper-Eddington bursts, the so-called "giant flares," of which the 5 March 1979 event (Mazets et al. 1979b) is the most famous example. Based on the few observed events, the SGRs appear to emit their giant flares on a recurrence timescale of years to decades. They also exhibit softer quiescent X-ray emission with coherent pulsations at periods of 5–10 s.

The SGRs are generally thought to be young ($< 10^4$ yr) neutron stars (NSs) with extremely strong magnetic fields ($> 10^{14}$ G), i.e. magnetars (Duncan & Thompson 1992; Thompson & Duncan 1993). This belief has been motivated by their several associations with young supernova remnants (SNRs) or star-forming regions (Evans et al. 1980; Kulkarni & Frail 1993; Fuchs et al. 1999; Vrba et al. 2000), by the energetics and phenomenology of their giant flares (Paczyński 1992; Thompson & Duncan 1995), and by the detection of X-ray pulsations with relatively long (5–10 s) periods and large ($\sim 10^{-11}$ s s^{-1}) spin-down rates (e.g. Kouveliotou et al. 1998, 1999).

1.1. SGR 1900+14

Historically, multiple bursts from SGR 1900+14 gave the first hint of the existence of a new class of gamma-ray transients (Mazets et al. 1979a), suggesting that SGR 0526−66, source of the famous 5 March 1979 event, was not alone. Reactivation of SGR 1900+14 in 1992 (Kouveliotou et al. 1993) led to follow-up observations that associated the burst source with a soft, persistent X-ray source (Vasisht et al. 1994; Hurley et al. 1996) and, possibly, an SNR 12 arcmin distant (G42.8+0.6; Vasisht et al. 1994). On 27 August 1998, a giant flare with strong 5 s pulsations was detected by several spacecraft (Hurley et al. 1999a); this flare remains the strongest gamma-ray event (in peak flux and fluence) detected to date from any cosmic source apart from the Sun. Arrival-time localization (Hurley et al. 1999b) identified SGR 1900+14 as the source, and prompt radio observations detected a fading, non-thermal radio source (Frail et al. 1999) coincident with the quiescent X-ray source, a 5.17-s pulsar (Hurley et al. 1999c). Timing analyses of the quiescent X-ray emission soon revealed that the pulsar was spinning down in magnetar-like fashion (Kouveliotou et al. 1999). Observations of the source in the aftermath of the flare demonstrated, in addition, a short-term (∼hours) increase in spin-down rate (Palmer 2001) and associated deviations from simple spin-down (Woods et al. 1999b). The radio detection provided the highest-accuracy position for SGR 1900+14 (current as of August 1998): $\alpha_{2000} = 19^{\rm h}07^{\rm m}14\overset{\rm s}{.}33$, $\delta_{2000} = +09^\circ 19' 20\overset{''}{.}1$, with uncertainty $\pm 0\overset{''}{.}15$ in each coordinate (Frail et al. 1999).

The precise localization of SGR 1900+14 has since enabled further observations at all wavelengths. Lorimer & Xilouris (2000) and Kulkarni et al. (2001b) have raised questions

about the association of SGR 1900+14 with G42.8+0.6; Vrba et al. (2000) have proposed instead an association of SGR 1900+14 with an embedded cluster of high-mass stars, 12 arcsec from the source, that is probably located at a distance of 12–15 kpc. Additional follow-up observations in the infrared (Eikenberry & Dror 2000), optical, and radio (Kaplan et al. 2001b) have been undertaken; although these have not revealed any point-source candidate counterparts to date, the upper limits on persistent emission in the IR band can now constrain accretion disk models for the source (c.f. van Paradijs et al. 1995; Marsden et al. 2001), as discussed by Kaplan et al. (2001a).

On 2001 April 18.33, the *Beppo-SAX* and *Ulysses* satellites detected a second giant flare from SGR 1900+14 (Guidorzi et al. 2001; Hurley et al. 2001) with duration ~ 40 s, 25-100 keV fluence $\sim 2.6\times10^{-4}$ ergs cm^{-2}, and peak flux over 0.5 s of $\sim 1.7\times10^{-5}$ ergs cm^{-2} s^{-1} ($\sim 25\times$ less fluence and $\sim 200\times$ lower peak flux than the flare of August 1998). In response we initiated observations of SGR 1900+14 with the *Chandra X-ray Observatory*, *Rossi X-ray Timing Explorer*, and Very Large Array, seeking to investigate the numerous transient phenomena that have been associated with the giant flares. Kouveliotou et al. (2001) have pursued a similar agenda with their overlapping set of observations.

2. Observations & Analysis

Our program sought to probe the immediate aftermath of the flare with sensitive X-ray spectral, X-ray timing, and radio imaging observations. These observations also allow us to investigate the nature of SGR 1900+14.

2.1. Radio

We observed the position of the radio transient associated with the August 1998 giant flare (Frail et al. 1999) from SGR 1900+14 with the Very Large Array[1] (VLA) in its "B" configuration on a number of occasions, as part of our regular observing program and using observing time donated by others. A log of these observations is found in Table 4. The data were taken in continuum mode with 2×50 MHz bandwidth. They were reduced and calibrated using standard procedures in `AIPS`, and then imaged with the `IMAGR` task. This yielded beam sizes of $\approx 4\farcs5$ and $0\farcs8$ at 1.4 GHz and 8.4 GHz, respectively. We did not detect

[1]The VLA is operated by the National Radio Astronomy Observatory, which is a facility of the National Science Foundation operated under cooperative agreement by Associated Universities, Inc.

a source in any of the observations, giving the 3σ upper limits plotted in Figure 1.

2.2. X-ray

We observed SGR 1900+14 with the *Chandra X-ray Observatory* on two occasions after the flare, beginning on 2001 April 22.19 UT and 2001 April 30.97 UT, with durations of 20.8 ks and 18.9 ks respectively, as part of the Director's Discretionary Time allocation, with no proprietary data rights period. Both observations were taken in continuous-clocking mode with the aimpoint on the backside-illuminated ACIS S-3 detector. This gave us a time resolution of 2.85 ms and mitigated the effects of photon pileup for the persistent emission, as well as for bursts of modest size, while sacrificing one dimension of spatial information.

The two *Chandra* observations were coordinated with two observations of the *Rossi X-ray Timing Explorer* (*RXTE*) whose data were also made immediately public. Due to a change in *Chandra* planning that was not mirrored by *RXTE*, the first *Chandra* observation occurred one day after the first *RXTE* observation. The second *RXTE* and *Chandra* observations overlapped as planned. The *RXTE* observations began at 2001 Apr 21.32 UT and 2001 Apr 30.99 UT, lasted for 15.2 and 15.6 ks respectively, and had total good-time intervals, after screening of Earth occults and intervals of high electron background, of 9.6 and 8.9 ks respectively.

Chandra data were processed, for the most part, according to standard CXC procedures. First we examined the lightcurve of a background region for high-background intervals; none were identified. We then extracted events recorded by the ACIS S-3 detector and restricted to the energy range 0.3–10 keV. We barycentered this data using the `axbary` tool with a preliminary *CXO* ephemeris. We extracted the events from a region 10 pixels ($\approx 5''$) wide. This region gives source count rates of 0.620 ± 0.006 s^{-1} and 0.534 ± 0.005 s^{-1} for the two observations. For precision timing analyses we were forced to account separately for the charge-transfer time, that is, the approximately 4 s it takes for the charge packets produced by each X-ray photon from the source to be read out from the center of the ACIS-S3 chip. We made this correction in two different ways: first, by following an approximate prescription related to us by the *Chandra* X-ray Center Helpdesk staff; and second, by executing a shell script provided to us by Allyn Tennant of the Marshall Space Flight Center[2]. Results of the two approaches were identical; however, we note that the latter approach is superior in that it incorporates higher-order corrections for the dither-motion and flexure of the observatory over the course of the observation; these corrections will make a difference for analyses

[2]Script available at `http://wwwastro.msfc.nasa.gov/xray/ACIS/cctime/`

requiring significantly more precision than ours.

RXTE realtime data were processed according to the protocols described on the *RXTE* web site[3]; note that the *RXTE* pointing was offset from SGR 1900+14 by 20 arcmin to reduce contamination from the bright source GRS 1915+105, resulting in a factor of 1.5 decrease in count rates relative to direct-pointing observations due to reduced collimator efficiency. The spectrum was (particle) background-dominated at high energies, so timing analyses were performed on 2–60 keV data only.

2.2.1. Phase-Averaged Spectral Analysis

Our spectral analysis focused first on the *Chandra* data. We extracted the events in a large background region and used the CXC tool `psextract` to bin the source and background event data and generate the appropriate response files. We then fit the data using the `XSPEC` and `Sherpa` packages independently. As a caveat to the results reported below, we note that the continuous-clocking mode of ACIS has not yet been independently calibrated for spectral purposes; our analysis depends on the calibration of the timed-exposure "Faint" mode of ACIS S-3, which telemeters an equivalent quantity of information about each event (3×3 pixel islands). To the extent that photon interaction times in the CCD substrate are negligible compared to the CC single-row clocking time of 2.85 ms, we expect this calibration to be accurate.

Pure blackbody fits (with interstellar absorption) were unable to fit the spectra, indicating that a harder spectral component was required. Single-temperature thermal bremsstrahlung models were able to fit the data but only with plasma temperatures so high that the resulting spectra in the ACIS 0.2–10 keV range were little different from simple power laws; thus a power-law component became our starting point for the fits.

Single power-law (PL-only) models (with hydrogen absorption) were able to fit the data satisfactorily (Table 1). However, the resulting power-law indices are quite steep (>2.5), requiring high column densities and implying relatively low high-energy fluxes, especially when extrapolated to the *RXTE* band. Adding a blackbody component to the models remedied these possible defects, but could not be justified in a strict statistical sense (F-test probability of 62% for the additional parameters in the joint fit). To determine, then, whether the PL-only fits were a realistic description of the spectra, we examined the high-energy range of the data in greater detail. As shown in Fig. 2, above 5 keV the effects of

[3] `http://heasarc.gsfc.nasa.gov/docs/xte/recipes/cook_book.html`

interstellar absorption, or of any ≈0.5 keV blackbody, on the spectrum are negligible.

We therefore executed our power-law plus blackbody (PL+BB) fits in the following manner. First, we fit a PL to the data in the 5–10 keV range. At these energies a BB component is superfluous, and fits are insensitive to the precise amount of interstellar absorption. As indicated in Table 1, the PL indices for these 5–10 keV fits are significantly harder than those for the 1–10 keV PL-only fits: the difference for the first observation is 2.7σ and for the second 1.8σ, giving an overall significance for the distinction of 3.8σ. We then froze the PL parameters at their best fit 5–10 keV values, added a soft (~ 0.5 keV) BB plus interstellar absorption, and fit the full 1–10 keV dataset, allowing the BB parameters as well as N_H to vary – note, however, that N_H was forced to be the same for both epochs. This fit, with fixed PL normalizations and power-law indices, required a soft (BB) component at very high confidence. After making this constrained fit, we freed all parameters and fit a final time. The results of this final fit are given in Table 1, along with the results of the 1–10 keV and the 5–10 keV PL-only fits.

Our best-fit PL+BB models are plotted in Figure 3 (PL-only fits appear indistinguishable). We note that while *Chandra* does not have sufficient sensitivity at high energies (> 10 keV) to discriminate directly between the PL+BB and PL-only models, other satellites, including *RXTE* and *Beppo-SAX*, do; see Section 2.2.2 for our approach on this point. Therefore we also quote in Table 1 the 2–10 keV fluxes from the models, as appropriate for comparison with other satellites. While the 0.5–10 keV fluxes are very similar for the PL or PL+BB models, there are significant differences in the absorbed 2–10 keV fluxes of the two models.

No narrow spectral features are apparent. The absorption "feature" near 2 keV is likely to be an instrumental artifact (Si)[4]. The 2-σ upper limit on the flux of a persistent 0.2-keV FWHM emission line in the 5–7 keV range (c.f. Strohmayer & Ibrahim 2000) is 10^{-5} photons cm^{-2} s^{-1}, corresponding to an equivalent width at 6.5 keV of less than 150 eV; narrower lines with similar equivalent widths would have been readily apparent in the data.

We attempted to extract time-averaged spectral information from the *RXTE* data as well. However, with the faintness of the source (which we estimate from our *Chandra* fits at 2 c s^{-1} for three active PCUs of the *RXTE* PCA), the high background (≈100 c s^{-1}) – some of which is likely due to unresolved sources near the Galactic plane – and the non-imaging nature of the PCA, we have been unable so far to obtain meaningful results.

[4]See `http://asc.harvard.edu/cal/Links/Acis/acis/Cal_prods/matrix/notes/Fl-esc.html`

2.2.2. Phase-resolved spectral analysis

To perform a phase-resolved spectral analysis we divided the *Chandra* events into six phase bins, according to the best fit period for each observation. We constructed a spectrum for each spectral bin independently. With the reduced counts of the phase-binned spectra we were unable to discriminate between multicomponent spectral models and fit a PL only, fixing N_H to the best-fit value for the PL-only fits to the phase-averaged data set (2.75×10^{22} cm^{-2}; see Table 1). Whether or not this model is accurate, the fits illustrate the gross variations in spectral shape (hardness) with phase exhibited by the source. We see in Figure 4 that there are moderate variations across the phase, with the beginning of the cycle harder than the end, and with an additional softening at pulse-maximum. The shape remains similar over the two observations.

As mentioned previously, we were not able to make a direct comparison with the *RXTE* spectral results due to unresolved background emission in the *RXTE* data that corrupted the absolute flux levels. However, we were able to compare the fluxes for pulse ON−OFF. Specifically, we extracted spectral datasets for the 1/3 of the phase around the maximum (ON) and the minimum (OFF) of the pulse for both *Chandra* and *RXTE* for the second epoch of (overlapping) observations. Our goal was to use the two datasets in combination to make an independent test of the reasonability of the PL+BB fits.

For the *RXTE* data we fit the PCABACKEST-subtracted data in the 7–20 keV range for the ON and OFF datasets with a power-law plus ∼7 keV Gaussian. We are only interested in the flux difference between these fits so the exact parameterization here is not crucial; however, we do fix $N_{\rm H}$ in the fits to 2.0×10^{22} cm^{-2}, a reasonable value from the *Chandra* fits. We determined our uncertainties in the flux difference by exploring the parameter space near the minimum for the ON and OFF datasets, determining one-sigma flux errors for each, and combining these ON and OFF errors in quadrature. The *RXTE* fits, combined with this investigation of the errors, demonstrate an ON−OFF flux difference of $4.0 \pm 1.2 \times 10^{-12}$ erg cm^{-2} s^{-1} (7–20 keV).

When we fit the *Chandra* ON and OFF pulse data using a PL-only model, the best-fit power-law photon indices for the two datasets are quite similar, ≈ 2.8, and the best-fit flux difference in the extrapolated 7–20 keV band is 1.3×10^{-12} erg cm^{-2} s^{-1}. Investigating the parameter space defined by the ON and OFF power-law indices of the fit, which will have the largest effect on the extrapolated *RXTE* flux, we find that the maximum ON−OFF flux allowed by the PL-only models is 1.57×10^{-12} erg cm^{-2} s^{-1} (3-σ upper limit). This value is 2σ from the actual *RXTE* flux. By contrast, the PL+BB fits give an ON−OFF flux difference of $2.5 \pm 1.4 \times 10^{12}$ erg cm^{-2} s^{-1}, which is only 0.8σ different from the *RXTE* value.

We feel that the combined weight of the 5–10 keV *Chandra* fits and the 7–20 keV *RXTE*-*Chandra* ON−OFF fits demonstrates that the BB component of the spectral models is indeed required by the data. We note that Kouveliotou et al. (2001) reached the same conclusion by making fits to the summed spectrum of the two *Chandra* observations.

2.2.3. Bursts

A cursory examination of the *RXTE* data revealed several short (<0.25 s), intense (>30 c s^{-1} PCU^{-1}) bursts – as typical for SGRs – in each observation. We therefore made a systematic search for bursts in all data sets. We constructed a 1/8-s-resolution light curve for each observation and identified all bins with $>4\sigma$ fluctuations above background. These bursts, detected in one or two adjacent time-bins exclusively, are listed in Table 2. Since we do not make a detailed investigation of the burst spectra, burst fluences given in the table should be taken as suggestive only.

Exactly one burst is detected in the *Chandra* dataset. This event occurred at 2001 April 22.30, 9079.8 s after the start of the first observation, and contains ≈14 photons over 0.27 s for a count rate of ≈ 83 times the quiescent rate. This implies a 0.5–10 keV X-ray flux of $\approx 8 \times 10^{-10}$ ergs cm^{-2} s^{-1} (for either spectral model), and an unabsorbed flux of 1.9×10^{-9} ergs cm^{-2} s^{-1} (for the PL+BB model) or 3.6×10^{-9} ergs cm^{-2} s^{-1} (for the PL-only model).

All seven bursts detected during the second *RXTE* observation occurred during times of simultaneous observation by *Chandra*. Examination of the *Chandra* light curve reveals that several of these bursts were accompanied by a mild excess in the ACIS count rate. The excess *Chandra* counts at the times of the *RXTE* bursts provide an independent demonstration of the consistency of the absolute timing for both satellites, to a precision of $\lesssim$0.1 s. In the context of the *Chandra* continuous-clocking observation, this establishes the position of the source on-chip, along the Y axis, to $\lesssim$35 pixels, and the position of the source on-sky to $\lesssim$18 arcsec from its August 1998 VLA position (the assumed location for all timing analyses). We make a more precise determination of the two-dimensional source position below (Sec. 2.2.5).

2.2.4. Pulsations

Fourier power spectra of the two *Chandra* observations show a clear pulse peak at the location of the known 5.17 s period of SGR 1900+14 (Hurley et al. 1999c). To make a more

precise characterization of the pulse period and phase at the start of each observation, we performed a phase connection of the *Chandra* data; this also allowed us to test for variability of the pulse strength over the course of the observation. The phase connection procedure was implemented by dividing the observation into six sections and folding the data (a barycenter-corrected light curve with 1/8-s resolution) in each section about the pulse period. From the folded pulse profile we derived the phase at the start of each section, as well as a phase uncertainty that we determined by Monte Carlo simulation. The connection of these phases then provided us with the value and uncertainties for the observation's pulse period and starting pulse phase.

We find the pulse profile of the first *Chandra* observation to be largely sinusoidal. There is evidence, at the 2.9-σ level, for power at the first harmonic of the pulse period (twice the main pulse frequency); the harmonic power is $4.3^{+3.1}_{-1.8}$% the power at the fundamental if it is real. Any power at the second harmonic is less than 3.5% the power of the fundamental at 90%-confidence.

The pulse profile of the second *Chandra* observation has a first harmonic detected with >3-σ confidence. Its power is 10^{+7}_{-4}% the power at the fundamental, marginally consistent with results from the first observation. Any power at the second harmonic is less than 7.2% the power of the fundamental at 90%-confidence for this observation. Folded pulse profiles from the two *Chandra* observations are shown in Figure 5.

We also performed a phase connection on the data from the *RXTE* observations. The procedure was identical; however, we used a barycenter-corrected light curve of 1/8-s resolution divided into four sections. Uncertainties from this analysis were greater due to the much larger background in the *RXTE* data.

The results of our timing analysis are shown in Table 3. A Bayesian period-estimator (Gregory & Loredo 1992) analysis of the data yielded similar results. The pulsed signal did not show detectable variation in frequency or strength over the course of any observation, consistent with prior and contemporaneous reports (Woods et al. 2001) and with expectations for a slow pulsar such as SGR 1900+14. A global analysis of our results yields a period derivative for SGR 1900+14 of $\dot{P} = 9.2 \pm 9.7 \times 10^{-11}$ at the epoch of the first *RXTE* observation, MJD 52020.5, consistent with the more precise results of Woods et al. (2001). There are no significant variations of the strength or profile of the pulsations with energy for either *Chandra* observation.

2.2.5. Localization

The one-dimensional spatial profile is consistent at close radii with an unresolved source, having a Gaussian shape with $\sigma \approx 0\farcs3$ (c.f. Marshall et al. 2001). Kouveliotou et al. (2001) have pointed out that at larger radii (>5 arcsec) a scattering halo, the product of X-ray scattering off of interstellar dust, is apparent.

With only one dimension of spatial information, an individual observation does not give a precise two dimensional location (without highly precise timing information), but merely confines the source to a one-dimensional locus. We were able, however, to use the two observations together to obtain a two-dimensional localization as each observation was taken at a slightly different orientation, with roll angles differing by 4.8°. When the one-dimensional positions are combined, there is a quasi-elliptical region of overlap centered at $\alpha_{2000} = 19^{\rm h}07^{\rm m}14\fs362$, $\delta_{2000} = +09°19'20\farcs04$, with statistical 1-$\sigma$ error contours of semi-major axis $0\farcs28$, semi-minor axis $0\farcs01$, and position angle 73° East of North (Figure 6). This position has absolute systematic uncertainties of up to $1''$ due to *Chandra* aspect errors, but we have here assumed that the separate observations possess internally consistent aspect determinations to $\lesssim$0.1 arcsec; this agrees with our experience with other *Chandra* data sets. Under this assumption, the resulting localization is consistent to a high degree of accuracy with the position of the August 1998 radio transient (Frail et al. 1999).

3. Discussion

3.1. Radio

Frail et al. (1999) reported, following the giant August 1998 flare, the detection of a transient radio source. Their observations covered the time interval from 1 week to 1 month after the burst. The source was detected in the first observation, 1 week after the burst, and then declined over the course of the following four observations (9–30 d; Fig. 1). Thus – at least for this giant flare – the radio source appears to have peaked about a week after the burst and subsequently undergone a power-law decay.

For the April 2001 flare, we undertook VLA observations beginning 0.17 d after the event and ending almost two weeks later (Table 4). Despite our prompt radio observations, we did not detect a radio source comparable in strength to the August 1998 flare at any of our five epochs of observation.

The fluence of the August 1998 flare was 10^{-2} erg cm^{-2} (here we include the contribution to the fluence from the initial hard spike and the subsequent softer afterglow; Feroci et al.

2001). In contrast, the fluence of the April 2001 flare was 2.6×10^{-4} erg cm^{-2} (Hurley et al. 2001). The inferred peak flux of the transient radio source for the August 1998 flare was about 400 μJy in the 8.46-GHz band. If the radio flux is proportional to the energy released by the flare then we would expect a peak radio flux of 10 μJy in the same band some time $\sim$0.1–10 d after the current flare. In this context, as seen from Table 4 and Fig. 1, our failure to detect a transient radio source is not surprising.

We end by noting a possibly interesting point. The origin of the transient radio source from SGR outbursts is not well understood. It is clear that the radio emission is powered by the flare in some way. Could it be that the radio emission arises from internal shocks of the emitted particles? Alternatively, the radio emission could be from the shock of the ambient gas driven by the burst of particles (the "afterglow" model). In this context we note that the radio emission of the August 1998 flare appears to peak, in the 8.46-GHz band, one week after the burst, suggesting that the emission at this frequency was optically thick. If so, the flux at earlier epochs may well have been higher at higher frequency. One way to test this idea would be to observe the burst source at higher frequencies (>20 GHz) at early times. Observatories currently capable of the requisite sensitivity at these frequencies include the VLA, the Owens Valley Radio Observatory, and the James Clerk Maxwell Telescope (SCUBA).

3.2. X-ray

With our X-ray observations, we are able to establish that the X-ray source remains unresolved, in one dimension, even at *Chandra*'s extraordinary resolution. Our upper limit of 0.6 arcsec on the FWHM of any persistent extended emission translates into a physical extent of less than $0.015 d_5$ pc, where d_5 is the distance to the source divided by five kiloparsecs. Recent suggestions that SGR 1900+14 could be as distant as 15 kpc (Vrba et al. 2000) may relax this constraint somewhat, but in general the possibilities for localized plerionic emission (c.f. Gaensler 2001) seem remote at this point.

Using the two *Chandra* observations in concert we are able to derive a highly precise location for SGR 1900+14. Although the uncertain *Chandra* absolute aspect probably implies an uncertainty of $\sim$1 arcsec in this position, the best-fit location is less than 0.5 arcsec from the location of the August 1998 radio flare (Frail et al. 1999). Our limit on the proper motion of the source becomes relevant if one considers that SGR 1900+14 has been proposed to be associated with G42.8+0.6, 12 arcmin distant, and that the nominal spin-down age of SGR 1900+14 was measured, at least initially, to be just 700 yr (Kouveliotou et al. 1999). Taken at face value this would imply a proper motion of fully 1.0 arcsec per year, or 2.7 arcsec between August 1998 and May 2000, significantly exceeding our limit. The alternative

possibilities – that SGR 1900+14 is not associated with G42.8+0.6, or that SGR 1900+14 is significantly older than its spin-down age would imply – are consistent with our data.

Our X-ray spectral observations find the source initially in a state of enhanced X-ray luminosity relative to the quiescent-state observations of Woods et al. (1999a) and Woods et al. (2001). These past observations found the source at an unabsorbed 2–10 keV flux of $\approx 1 \times 10^{-11}$ erg cm^{-2} s^{-1} on two occasions, 1997 May and 2000 March. Our first observation finds the source at 20% greater flux, while the flux at the second observation is consistent with the quiescent value (Table 1). The fading nature of this excess emission is confirmed by reports of *Beppo-SAX* observations at earlier times (Feroci et al. 2001). Spectral parameters for the thermal component in the spectrum are consistent with values reported for the source in quiescence (Woods et al. 1999a, 2001; Perna et al. 2001), and despite the 20% decline in total X-ray flux between our two observations, fitted blackbody parameters show no significant variation – indicating that the variations in source flux are produced solely by the power-law component in the spectrum. Similar fading of the power-law component alone was observed in the wake of the August 1998 giant flare of the source (Woods et al. 1999a). This stability of the blackbody component of SGR 1900+14 has been cited as evidence in favor of the magnetar model for SGRs, with the blackbody produced by surface thermal emission and the power law produced in the magnetosphere by, e.g., inverse Compton effects (Woods et al. 1999a). This interpretation must be further strengthened by the observations reported here, as the stability of the blackbody component of SGR 1900+14 has now withstood two giant flares as well as substantial excursions in X-ray flux.

The X-ray spectrum of SGR 1900+14 thus provides an interesting link between the SGR population and the related population of anomalous x-ray pulsars (AXPs). The AXPs (see Mereghetti 2000) are a group of sources that emit steady, pulsed X-ray emission ($L_X \sim 10^{35}$ erg s^{-1}) with periods and spin-down rates similar to those of the SGRs; indeed, Thompson & Duncan (1996) used spin properties to argue that the SGRs and AXPs were related. However, these spin properties are also shared by a growing class of long-period radio pulsars (Kaspi et al. 1999) which seem otherwise unrelated to both the AXPs – showing no persistent bright X-ray emission (Pivovaroff et al. 2000) – and the SGRs – showing no bursting behavior. We must therefore require more evidence than similar spin properties to relate the SGRs and AXPs.

For some time the X-ray spectra of the two groups appeared to have important differences: the SGRs had relatively hard power-law spectra with photon indices $\Gamma \sim 2$ and negligible blackbody contributions (Hurley 2000), while the AXPs had softer spectra, with $\Gamma \sim 4$ and ~ 0.5 keV blackbodies contributing up to 70% of the X-ray flux (Mereghetti 2000). But this situation has been changing. Observations of the quiescent SGR 0526−66

found a photon index of 3.2 – closer to the nominal AXP index than to the that of the other SGRs – and possible evidence for a 0.5 keV blackbody (Kulkarni et al. 2001a). This may put the value of the photon index on a continuum related to burst activity and magnetic field geometry for both groups. Observations of SGR 1900+14 in quiescent and active states demonstrated the presence of an underlying ∼0.5 keV blackbody (Woods et al. 1999a, 2001). Updated spectral fits of archival *ASCA* data of SGRs and AXPs have shown that both groups seem to possess blackbody components whose fraction of the overall X-ray emission may constitute another unifying continuum (Perna et al. 2001). Spectral fits to the AXP 1E 1048.1−5937 show that it has a hard power-law component reminiscent of the SGRs (Kaspi et al. 2001). And finally, optical and infrared observations of SGRs (Kaplan et al. 2001a; Kulkarni et al. 2001b) and AXPs (Hulleman et al. 2000; Hulleman et al. 2000) have shown that the groups have similar X-ray-to-optical flux ratios, so that this ratio may be a distinguishing characteristic of the two, as a group (Hulleman et al. 2000). All of these findings have strengthened arguments for association between the AXPs and SGRs.

The blackbody component of the SGR 1900+14 spectrum, with $kT_{\rm BB} \approx 0.5$ keV and $R_{\rm BB} \approx 1.5 d_5$ km, has parameters that are similar to those of other isolated NS candidates (c.f. Verbunt et al. 1994). The relatively small emitting radius that we find, significantly smaller than the nominal ≈10 km-radius NS, is typically interpreted as either due to restricted emission from, e.g., the NS polar caps, or as the result of temperature-dependent opacity effects in the NS atmosphere (Rutledge et al. 1999; Perna et al. 2001). The latter scenario would allow for closer distances, lower surface temperatures, and, potentially, emission from the entire NS surface (Perna et al. 2001).

The absence of any narrow spectral features, to equivalent widths of less than 150 eV, is somewhat surprising given the detection by Strohmayer & Ibrahim (2000) of a strong, 400-eV equivalent width, ≈6.4-keV emission line in the *RXTE* spectrum of a 1998 August 29 burst of SGR 1900+14. Strohmayer & Ibrahim (2000) discuss two possible interpretations for the feature they observe: first, that it may result from fluorescence of relatively cool iron in the near vicinity of the NS; and second, that it may result from proton or alpha particle (He^4) cyclotron transitions in the SGR magnetosphere; these ions would have been liberated by the closely-preceding giant flare of 1998 August 27. However, if the line resulted from iron fluorescence then we would expect, with *Chandra*'s superior spectral resolution, to have substantially greater sensitivity with the current observations; note that the original emission feature was unresolved by the *RXTE* PCA. Similarly, if the line resulted from cyclotron emission by He^4 or H ions liberated by the preceding giant flare, then we would expect to observe such cyclotron emission in the wake of the current 2001 April 18 flare as well. Both of these scenarios would generate line emission in bursting and persistent source spectra alike. Our upper limits on the presence of any such feature in the persistent source

spectrum therefore seem to imply that the line emission is a function of the properties of (at least some of) the bursts alone.

4. Conclusions

We have observed the soft-gamma repeater SGR 1900+14 with high-resolution X-ray (*Chandra*, *RXTE*) and radio (VLA) observatories in the immediate aftermath of its 2001 April 18 giant flare. Our detailed study of the *Chandra* and *RXTE* X-ray spectra reveals the presence of an underlying thermal component in the spectrum. This thermal component, which we model as a blackbody, has an effective temperature of $kT_{\rm BB} \approx$0.5 keV and an effective blackbody radius of $R_{\rm BB} \approx 1.5 d_5$ km, where d_5 is the distance to the source divided by 5 kpc. This two-component PL+BB spectrum is strongly reminiscent of the spectra of the anomalous X-ray pulsars, further strengthening the association between these two intriguing classes of neutron star.

We detect enhanced, fading X-ray emission from the source, which is modulated by the source's known 5.17 s pulsations and, intermittently, by brief bursts of hard X-rays. Detailed studies of the pulsations will be able to determine whether any "glitch" of the source was associated with the April 18 flare. We are able to localize the source to $\lesssim$1 arcsec, and find that the current position remains consistent with the Frail et al. (1999) radio position from August 1998. This corresponds to an upper limit of $\lesssim$1 arcsec per year on any proper motion of SGR 1900+14.

The upper limits we derive on any radio emission from SGR 1900+14 in the 0.2–11 d following the flare may have implications for physical models of the post-flare radio emission. Higher-frequency (>20 GHz) observations in the immediate aftermath of future flares will provide stronger constraints for models that predict optically thick emission at lower frequencies.

The authors would like to thank Harvey Tananbaum, Jean Swank, and the *Chandra* and *RXTE* operations teams for their rapid and effective response to this target of opportunity. We would also like to thank G. Taylor, C. Carilli, T. Soifer, and J. Condon for donations of VLA time. DLK is supported by the Fannie & John Hertz Foundation.

REFERENCES

Duncan, R. C. & Thompson, C. 1992, ApJ, 392, L9

Eikenberry, S. S. & Dror, D. H. 2000, ApJ, 537, 429

Evans, W. D., Klebesadel, R. W., Laros, J. G., Cline, T. L., Desai, U. D., Teegarden, B. J., Pizzichini, G., Hurley, K., Niel, M., & Vedrenne, G. 1980, ApJ, 237, L7

Feroci, M., Hurley, K., Duncan, R. C., & Thompson, C. 2001, ApJ, 549, 1021

Feroci, M. et al. 2001, GCN 1055

Frail, D. A., Kulkarni, S. R., & Bloom, J. S. 1999, Nature, 398, 127

Fuchs, Y., Mirabel, F., Chaty, S., Claret, A., Cesarsky, C. J., & Cesarsky, D. A. 1999, A&A, 350, 891

Gaensler, B. M. 2001, in AIP Conference Proceedings, Vol. 565, Young Supernova Remnants, ed. S. S. Holt & U. Hwang (New York: AIP), 295

Gregory, P. C. & Loredo, T. J. 1992, ApJ, 398, 146

Guidorzi, C. et al. 2001, GCN 1041

Hulleman, F., van Kerkwijk, M. H., & Kulkarni, S. R. 2000, Nature, 408, 689

Hulleman, F., van Kerkwijk, M. H., Verbunt, F. W. M., & Kulkarni, S. R. 2000, A&A, 358, 605

Hurley, K. 2000, in Gamma-Ray Bursts: 5th Huntsville Symposium, ed. R. M. Kippen, R. S. Mallozi, & G. J. Fishman, 763, (astro-ph/9912061)

Hurley, K., Cline, T., Mazets, E., Barthelmy, S., Butterworth, P., Marshall, F., Palmer, D., Aptekar, R., Golenetskii, S., Il'Inskii, V., Frederiks, D., McTiernan, J., Gold, R., & Trombka, J. 1999a, Nature, 397, 41

Hurley, K., Kouveliotou, C., Woods, P., Cline, T., Butterworth, P., Mazets, E., Golenetskii, S., & Frederics, D. 1999b, ApJ, 510, L107

Hurley, K., Li, P., Kouveliotou, C., Murakami, T., Ando, M., Strohmayer, T., van Paradijs, J., Vrba, F., Luginbuhl, C., Yoshida, A., & Smith, I. 1999c, ApJ, 510, L111

Hurley, K., Li, P., Vrba, F., Luginbuhl, C., Hartmann, D., Kouveliotou, C., Meegan, C., Fishman, G., Kulkarni, S., Frail, D., Bowyer, S., & Lampton, M. 1996, ApJ, 463, L13

Hurley, K. et al. 2001, GCN 1043

Kaplan, D. L., Kulkarni, S. R., van Kerkwijk, M. H., Rothschild, R. E., Lingenfelter, R. L., Marsden, D., Danner, R., & Murakami, T. 2001a, ApJ, 556, 399

Kaplan, D. L., Kulkarni, S. R., van Kerkwijk, M. H., & Frail, D. A. 2001b, ApJ, submitted

Kaspi, V. M., Camilo, F., Lyne, A. G., Manchester, R. N., Bell, J. F., D'Amico, N., McKay, N. P. F., & Crawford, F. 1999, astro-ph/9912281

Kaspi, V. M., Gavriil, F. P., Chakrabarty, D., Lackey, J. R., & Muno, M. P. 2001, astro-ph/0107288

Kouveliotou, C., Dieters, S., Strohmayer, T., van Paradijs, J., Fishman, G. J., Meegan, C. A., Hurley, K., Kommers, J., Smith, I., Frail, D., & Murakami, T. 1998, Nature, 393, 235

Kouveliotou, C., Fishman, G. J., Meegan, C. A., Paciesas, W. S., Wilson, R. B., van Paradijs, J., Preece, R. D., Briggs, M. S., Pendleton, G. N., & Brock, M. N. 1993, Nature, 362, 728

Kouveliotou, C., Strohmayer, T., Hurley, K., van Paradijs, J., Finger, M. H., Dieters, S., Woods, P., Thompson, C., & Duncan, R. C. 1999, ApJ, 510, L115

Kouveliotou, C., Tennant, A., Woods, P. M., Weisskopf, M. C., Hurley, K., Fender, R. P., Garrington, S. T., Patel, S. K., & Göğüş, E. 2001, astro-ph/0107170

Kulkarni, S. R. & Frail, D. A. 1993, Nature, 365, 33

Kulkarni, S. R., Kaplan, D. L., Marshall, H. L., Frail, D. A., Murakami, T., & Yonetoku, D. 2001a, Nature, submitted

Kulkarni, S. R., Kaplan, D. L., Marshall, H. L., van Kerkwijk, M. H., & Frail, D. A. 2001b, in preparation

Lorimer, D. R. & Xilouris, K. M. 2000, ApJ, 545, 385

Marsden, D., Lingenfelter, R., Rothschild, R., & Higdon, J. 2001, ApJ, in press, (astro-ph/9912207)

Marshall, H. L., Rutledge, R., Fox, D. W., Miller, J. M., Guerriero, R., Morgan, E., van der Klis, M., Bildsten, L., Dotani, T., & Lewin, W. H. G. 2001, AJ, in press, preprint (astro-ph/0103203)

Mazets, E. P., Golenetskij, S. V., & Guryan, Y. A. 1979a, Soviet Astronomy Letters, 5, 343+

Mazets, E. P., Golentskii, S. V., Il'inskii, V. N., Aptekar', R. L., & Guryan, I. A. 1979b, Nature, 282, 587

Mereghetti, S. 2000, in The Neutron Star - Black Hole Connection, ed. V. Connaughton, C. Kouveliotou, J. van Paradijs, & J. Ventura (NATO Advanced Study Institute), (astro-ph/9911252)

Paczyński, B. 1992, Acta Astronomica, 42, 145

Palmer, D. M. 2001, in Soft Gamma Repeaters: The Rome 2001 Mini-Workshop, ed. M. Feroci & S. Mereghetti, astro-ph/0103404

Perna, R., Heyl, J., Hernquist, L., Juett, A., & Chakrabarty, D. 2001, ApJ, in press, (astro-ph/0103273)

Pivovaroff, M. J., Kaspi, V. M., & Camilo, F. 2000, ApJ, 535, 379

Rutledge, R. E., Bildsten, L., Brown, E. F., Pavlov, G. G., & Zavlin, V. E. 1999, ApJ, 514, 945

Strohmayer, T. E. & Ibrahim, A. I. 2000, ApJ, 537, L111

Thompson, C. & Duncan, R. C. 1993, ApJ, 408, 194

—. 1995, MNRAS, 275, 255

—. 1996, ApJ, 473, 322

van Paradijs, J., Taam, R. E., & van den Heuvel, E. P. J. 1995, A&A, 299, L41

Vasisht, G., Kulkarni, S. R., Frail, D. A., & Greiner, J. 1994, ApJ, 431, L35

Verbunt, F., Belloni, T., Johnston, H. M., van der Klis, M., & Lewin, W. H. G. 1994, A&A, 285, 903

Vrba, F. J., Henden, A. A., Luginbuhl, C. B., Guetter, H. H., Hartmann, D. H., & Klose, S. 2000, ApJ, 533, L17

Woods, P. M., Kouveliotou, C., Göğüş, E., Finger, M. H., Swank, J., Smith, D. A., Hurley, K., & Thompson, C. 2001, ApJ, 552, 748

Woods, P. M., Kouveliotou, C., van Paradijs, J., Finger, M. H., & Thompson, C. 1999a, ApJ, 518, L103

Woods, P. M., Kouveliotou, C., van Paradijs, J., Finger, M. H., Thompson, C., Duncan, R. C., Hurley, K., Strohmayer, T., Swank, J., & Murakami, T. 1999b, ApJ, 524, L55

Woods, P. M. et al. 2001, GCN 1056

This preprint was prepared with the AAS LaTeX macros v5.0.

Table 1. Summary of 0.5–10 keV spectral fits to *Chandra* data.

Parameter	PL		5–10 keV PL		PL+BB	
	Obs 1	Obs 2	Obs 1	Obs 2	Obs 1	Obs 2
N_H (10^{22} cm^{-2})[a]	2.75(5)		···		2.3(1)	
PL Index Γ	2.72(5)	2.82(5)	1.9(3)	2.1(4)	2.0(2)	1.9(3)
PL Norm[b]	0.0131(8)	0.0126(8)	0.003(1)	0.003(2)	0.004(1)	0.003(1)
PL Flux[c]	9.2	7.6	···	···	7.9	6.3
BB kT (keV)	···	···	···	···	0.52(3)	0.49(3)
BB Norm[d]	···	···	···	···	0.008(2)	0.011(3)
BB Flux[c]	···	···	···	···	1.8	1.8
Total Flux[c]	9.2	7.6	···	···	9.7	8.1
Unabs. Flux[c]	42.6	39.5	···	···	23.1	19.5
2–10 keV Flux[c]	8.5	6.9	···	···	9.0	7.5
Unabs. 2–10 keV Flux[c]	11.7	9.7	···	···	11.6	9.6
χ^2	279.8	227.5	32.8	25.2	276.2	220.7
DOF	318	287	59	44	318	288
χ^2/DOF	0.88	0.84	0.56	0.57	0.87	0.77
Total χ^2/DOF[e]	0.84		0.56		0.82	

[a]Held constant over the two observations for a given model.

[b]In units of photons cm^{-2} s^{-1} keV^{-1} at 1 keV.

[c]All fluxes are 0.5–10 keV, absorbed, unless otherwise specified; flux units are 10^{-12} erg cm^{-2} s^{-1}.

[d]In units of $0.44(R_{10}/d_5)^2$, where $R = 10R_{10}$ km is the source radius.

[e]Total reduced χ^2 for a model, incorporating both observations.

Note. — Number in parentheses is 1-σ uncertainty on last digit.

Table 2. Observed Bursts

Date / Inst.	Time (TDB)	Counts (raw)	Fluence ($\times 10^{-11}$ cgs)
21 April *RXTE* (3)	08:05:41.38	20	6.3
	08:08:56.88	31	9.9
	08:34:41.88	30	9.6
	08:34:58.51	38	12.2
	08:38:45.25	166	52.7
	08:42:18.13	27	8.6
	08:42:19.01	80	25.3
	08:45:50.26	65	20.7
21 April *RXTE* (4)	09:49:38.48	17	4.0
	09:50:26.86	18	4.2
	10:17:23.61	31	7.5
	10:22:26.23	22	5.2
21 April *RXTE* (2)	11:19:11.83	150	71.3
22 April *Chandra*	07:18:00.30	10	36.5
1 May *RXTE* (4)	01:49:06.89	65	15.4
	02:16:55.26	28	6.7
	02:35:08.01	16	3.8
	02:35:43.39	19	4.4
	02:36:56.64	15	3.5
	02:37:28.51	18	4.3
	02:37:32.64	16	3.9
1 May *RXTE* (3)	03:36:40.97	21	6.7
	04:01:26.22	113	35.9

Note. — Numbers in parentheses for *RXTE* observations indicate the number of active PCUs at the time of observation. Times are corrected to the solar-system barycenter (TDB). Estimated fluences in units of 10^{-11} erg cm^{-2} are calculated using the following conversion factors: 1 *RXTE* c PCU^{-1} $\approx 9.5 \times 10^{-12}$ erg cm^{-2} (7–20 keV); 1 *Chandra* ACIS c $\approx 3.7 \times 10^{11}$ erg cm^{-2} (0.1–11 keV).

Table 3. Pulse Timing Analysis

Mission	Epoch (MJD)	Phase (cyc.)	Pulsations Period (s.)	Strength (%rms)
RXTE	52020.5	0.76(9)	5.17274(22)	···
Chandra	52021.25	0.84(2)	5.172908(40)	16.2(9)
Chandra	52030.0	0.46(2)	5.172947(65)	13.4(11)
RXTE	52030.0	0.62(9)	5.17321(21)	···

Note. — Times are corrected to the solar-system barycenter (TDB); MJD is JD $- 2,400,000.5$. Phases reported refer to the phase of the sine wave at the fundamental frequency. Uncertainties in the last significant digit(s) are shown in parentheses. RMS pulse strengths have been corrected for background and include the contributions of the fundamental and first harmonic power.

Table 4. Summary of VLA Observations

Date of Observation (UT)	Days after Flare	Frequency (GHz)	Duration (min)	rms (μJy)
2001 Apr 18.58	0.17	8.4	15	40
2001 Apr 20.52	2.11	8.4	15	40
2001 Apr 20.53	2.12	1.4	15	200
2001 Apr 21.53	3.12	8.4	15	40
2001 Apr 24.50	6.09	8.4	60	20
2001 Apr 29.58	11.2	8.4	15	40

Note. — All observations were in B configuration.

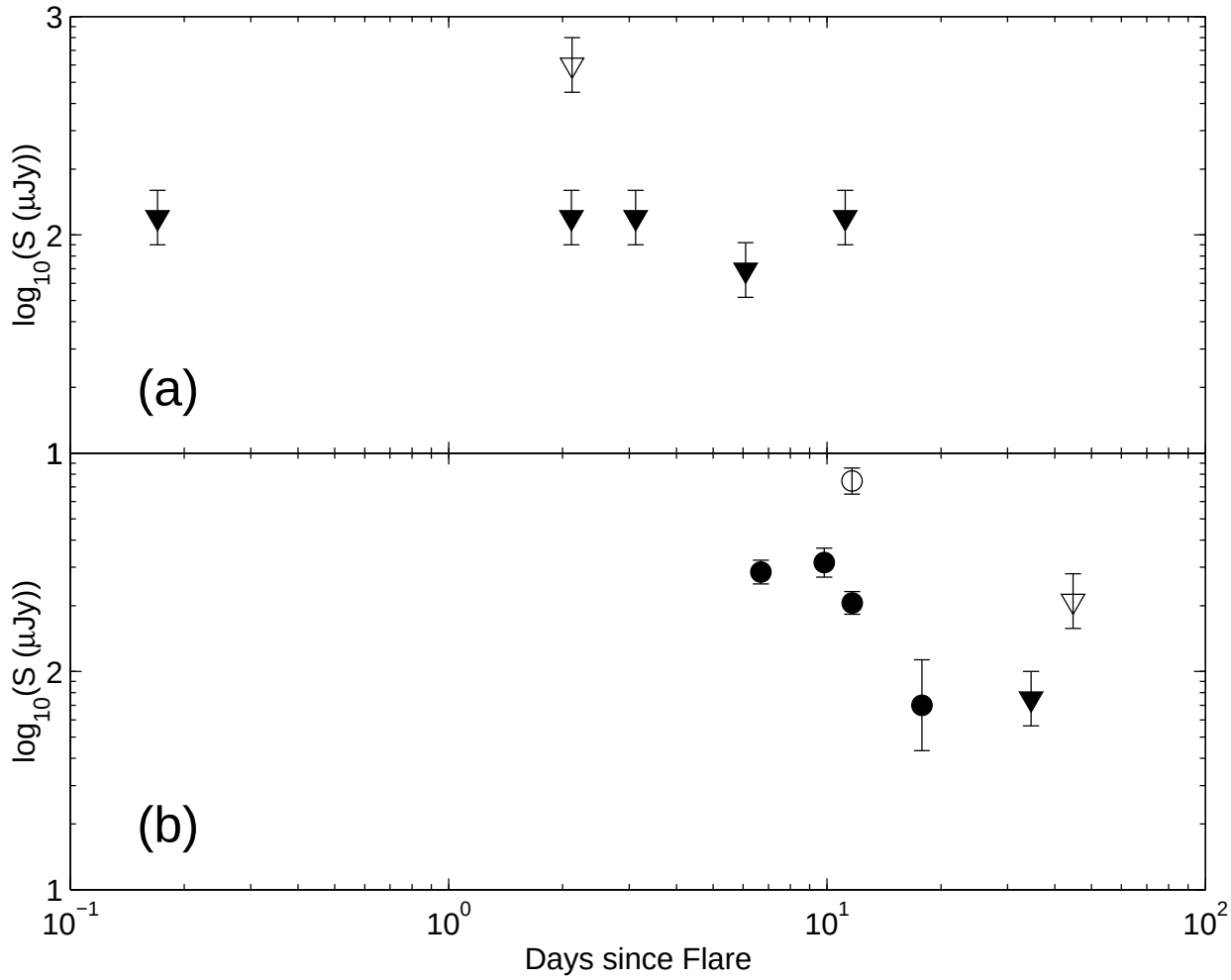

Fig. 1.— VLA radio observations of SGR 1900+14 in the aftermath of (a) the current flare; and (b) the August 1998 flare (Frail et al. 1999). Detections are plotted as circles and upper limits as triangles; corresponding radio frequencies are 1.4 GHz (open symbols) and 8.4 GHz (filled symbols). Upper limits are 3σ.

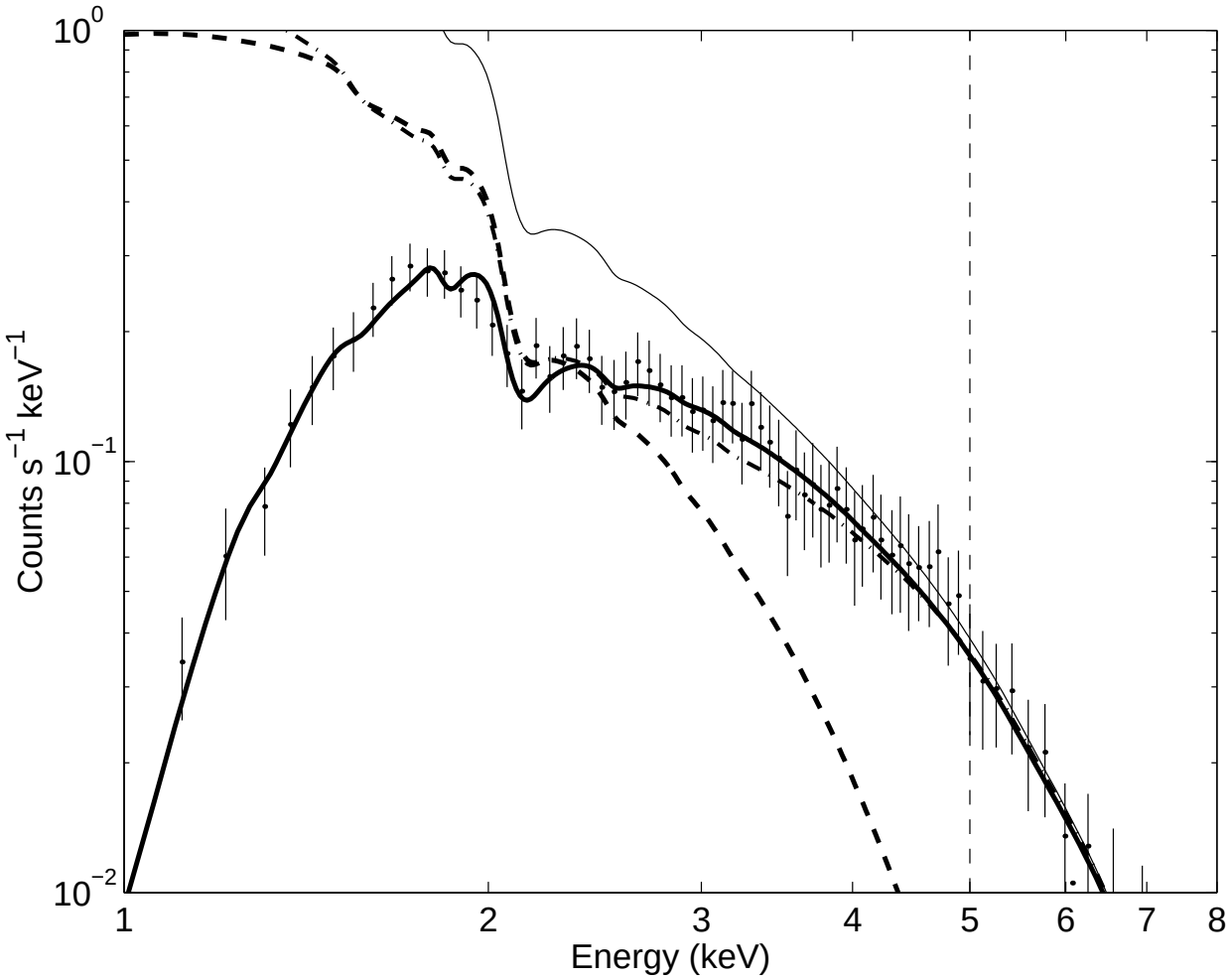

Fig. 2.— *Chandra* spectrum of SGR 1900+14 for the 2001 April 30 observation, illustrating the contributions of various spectral components to the final fit. Plotted are: the data (points, with error bars); the best-fit PL+BB model (thick line); its unabsorbed PL and BB components (dashed and dash-dotted lines, respectively); and an unabsorbed power-law fit to the 5–10 keV data only (thin solid line). Above 5 keV (dashed vertical line) the unabsorbed power-law is indistinguishable from the fully absorbed PL+BB model. This indicates that the region above 5 keV will provide the best measurement of the power-law index for the fit.

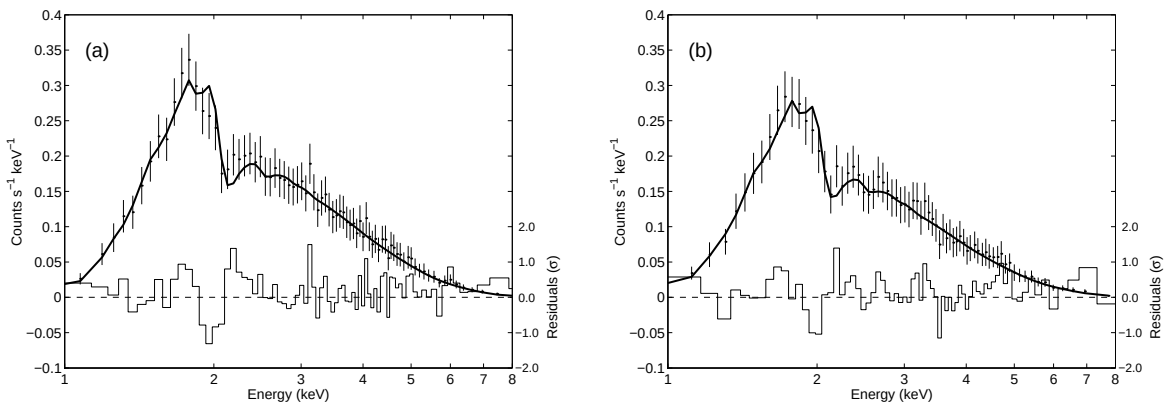

Fig. 3.— *Chandra* spectra of SGR 1900+14 for the (a) 2001 April 22 observation; and (b) 2001 April 30 observation. Plotted are data (points) and best-fit PL+BB models (thick lines). Residuals are plotted as the thin lines below the spectra (right axis for scale). The data have been adaptively binned to have ≈ 60 counts per bin. The PL fits are visually similar (see Table 1).

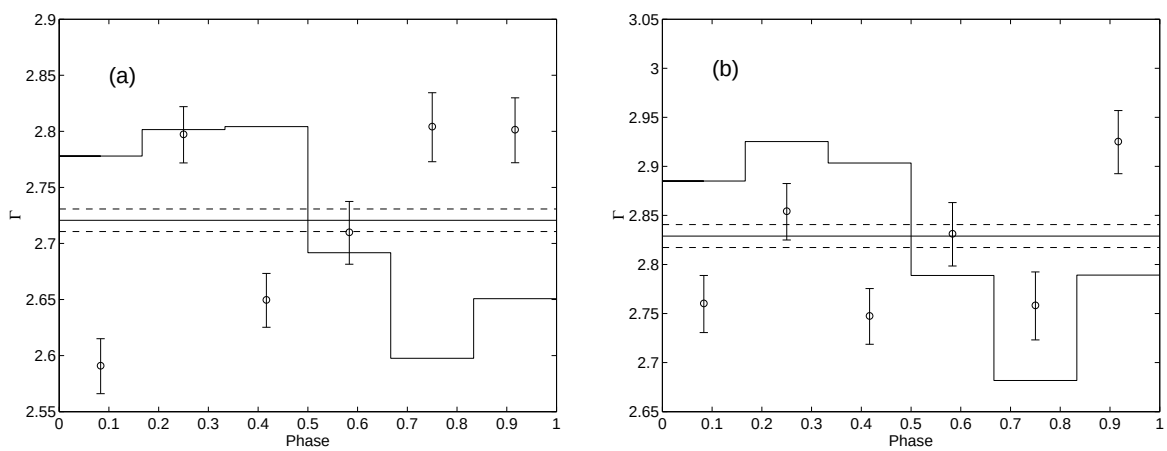

Fig. 4.— Variation of the best-fit power-law index Γ with pulse phase for the (a) 2001 April 22 observation; and (b) 2001 April 30 observation. The best-fit value of $N_H = 2.75 \times 10^{22}$ cm^{-2} derived from the phase-averaged spectral analysis was used for all of the fits (see Table 1). The phase-average value of Γ for each observation is plotted as the line across the middle, with $\pm 1\sigma$ errors given by the dotted lines. The corresponding 0.3–10 keV pulse profiles are also overplotted, with arbitrary scale.

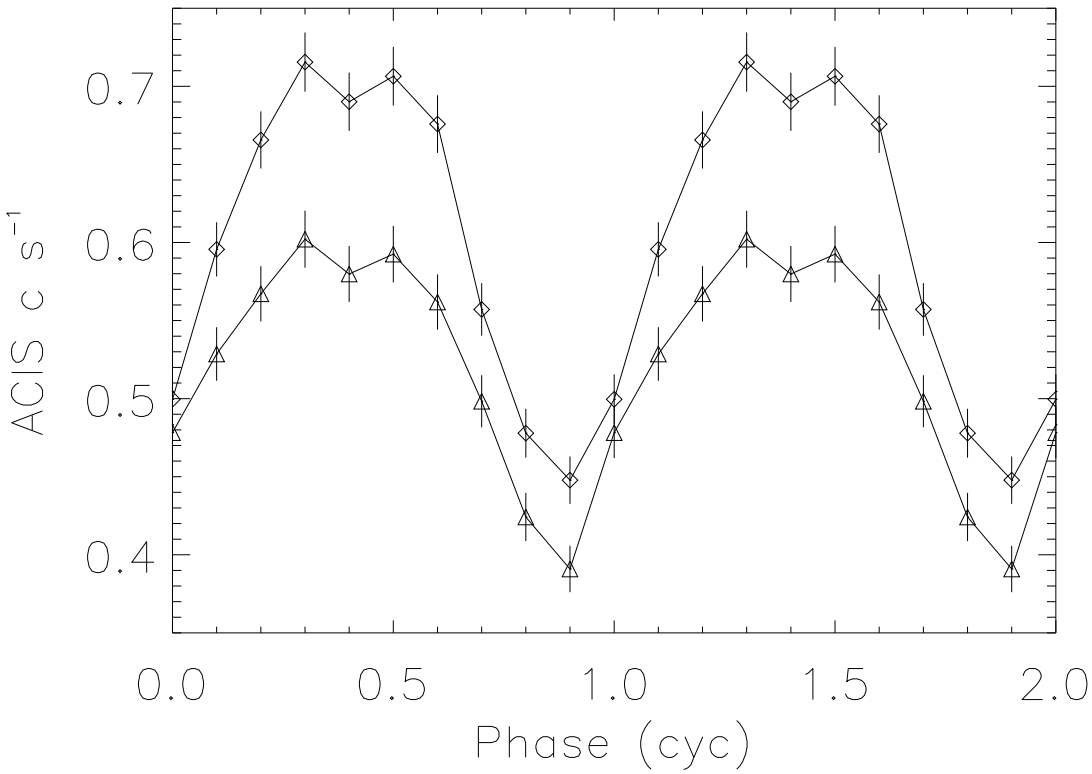

Fig. 5.— Folded pulse profiles from the two *Chandra* observations (first epoch: diamonds; second epoch: triangles; profiles are plotted twice for clarity). At the time of the second observation, SGR 1900+14 was exhibiting less flux, and, possibly, weaker modulation of the pulse signal. Both pulse profiles are highly sinusoidal, with ∼5% harmonic content.

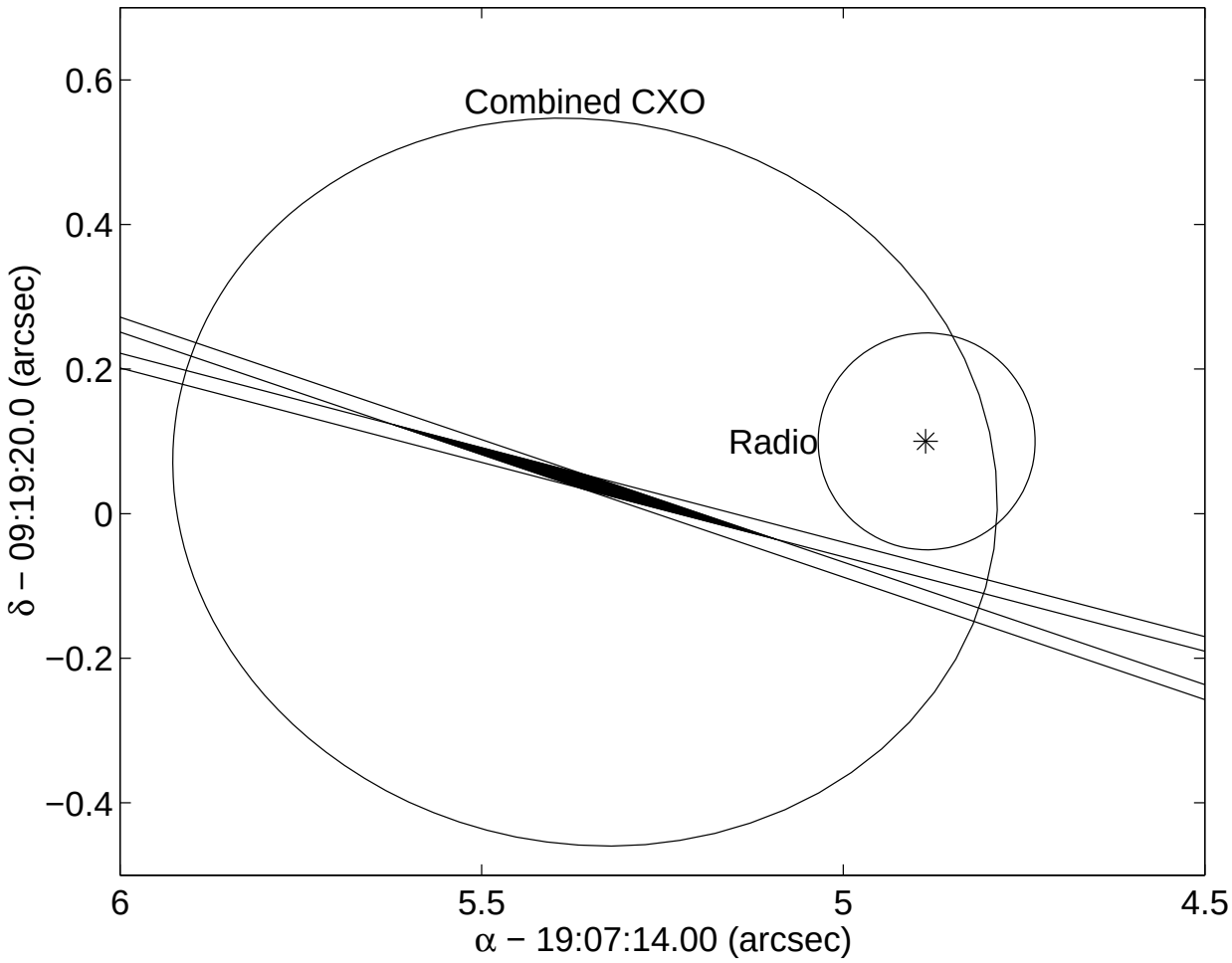

Fig. 6.— Two-dimensional localization of SGR 1900+14. The lines are the localizations for each individual X-ray observation, with statistical errors of $\sim 0\farcs02$ for each. The shaded region is the intersection of the two localizations, and represents the best-fit position from the *Chandra* data. The asterisk and circle marked "Radio" gives the position from Frail et al. (1999) with its associated $0\farcs15$ uncertainty. The ellipse around the X-ray position incorporates a $0\farcs5$ systematic error, identical for the two observations, arising from the uncertain absolute aspect of *Chandra*; this may be an underestimate.